Crystal Structures, Anisotropic Growth, and Optical Properties: Controlled Synthesis of Lanthanide Orthophosphate One-Dimensional Nanomaterials

Ruoxue Yan, Xiaoming Sun, Xun Wang, Qing Peng, and Yadong Li*[a]

Abstract: The fundamental understanding of the relationship between crystal structure and the dynamic processes of anisotropic growth on the nanoscale, and exploration of the key factors governing the evolution of physical properties in functional nanomaterials, have become two of the most urgent and challenging issues in the fabrication and exploitation of functional nanomaterials with designed properties and the development of nanoscale devices. Herein, we show how structural and kinetic factors govern the tendency for anisotropic growth of such materials under hydrothermal conditions, and how the crystal structure and morphology influence the optical properties of Ln^{3+}-doped nanocrystals. The synthesis of phase-pure and single-crystalline monoclinic, hexagonal, and tetragonal one-dimensional $LnPO_4$ nanostructures of different aspect ratios by means of kinetically controlled hydrothermal growth processes is demonstrated. It is shown that the tendency for anisotropic growth under hydrothermal conditions can be enhanced simply by modifying the chemical potentials of species in the reaction solution through the use of carefully selected chelating ligands. A systematic study of the photoluminescence of various Eu^{3+}-doped lanthanide phosphates has revealed that the optical properties of these nanophosphors are strongly dependent on their crystal structures and morphologies.

Keywords: hydrothermal synthesis · lanthanides · nanostructures · orthophosphates · photoluminescence

Introduction

Nanostructures, which have received wide recognition for their novel size- and shape-dependent properties, as well as their unique applications that complement those of their bulk counterparts, have been extensively investigated for over a decade.[1–5] The generation of such small structures is essential to the advance of many areas of modern science and technology, and a number of physical- and chemical-based synthetic methodologies have hence been developed.[6–12] However, the fabrication of a vast diversity of nanomaterials with well-controlled dimensionality, shape, phase purity, chemical composition, and desired properties remains as one of the most challenging issues faced by synthetic inorganic chemists.[13] Solutions to these challenges require a detailed, fundamental understanding of the nature of different crystal structures and of the dynamic processes governing the nucleation and growth of nanocrystals in various synthetic systems, as well as of the key factors that determine the evolution of physical properties in functional nanomaterials.[13] Unfortunately, although some recent studies have provided some insight into the factors that control the selective growth and ultimately determine the shape of nanocrystals,[14–18] systematic and detailed studies of this type are still very limited.

Recently, lanthanide compounds have attracted increased interest because of their wide applicability in magnets, phosphors, catalysts, biochemical probes, and medical diagnostics.[19,20] More importantly, we have realized, based on our previous work,[21,22] that for families of lanthanide compounds that share a common anion, such as LnF_3 or $Ln(OH)_3$, both the crystal structures and physical properties may vary gradually on ascending the series as a result of the lanthanide contraction. Such families therefore provide a framework for the systematic study of the interplay between crystal structure, anisotropic growth of nanocrystals, and their physical properties.

One of these ideal model systems comprises the lanthanide orthophosphates, which, in addition to their wide appli-

[a] R. Yan, Dr. X. Sun, Dr. X. Wang, Dr. Q. Peng, Prof. Y.-D. Li
Department of Chemistry and the Key Laboratory of Atomic and Molecular Nanosciences (National Center for Nanoscience and Nanotechnology, Ministry of Education, China), Tsinghua University
Beijing, 100084 (P. R. China)
Fax: (+86) 10-6278-8765
E-mail: ydli@tsinghua.edu.cn

Supporting information for this article is available on the WWW under http://www.chemeurj.org/ or from the author.

 DOI: 10.1002/chem.200400649

cations,[23] are rich in polymorphs: monazite, xenotime, rhabdophane, weinschenkite, and orthorhombic.[24] Various $LnPO_4$ nanostructures, including redispersible $LnPO_4$ nanoparticles and $LnPO_4{\cdot}n\,H_2O$ nanowires/nanorods of some highly anisotropic polymorphs, have thus far been synthesized.[23–29] Despite these efforts, important issues, such as the fundamental relationship between crystal structure and the dynamic processes of anisotropic growth on the nanoscale, as well as exploration of the key factors governing the evolution of physical properties, are still in need of in-depth investigation.

Herein, we show how structural and kinetic factors govern the tendency for anisotropic growth and the shape evolution of $LnPO_4$ polymorphs on the nanoscale, and how the crystal structure and morphology influence the optical properties of Ln^{3+}-doped $LnPO_4$ nanocrystals. The synthesis of phase-pure and single-crystalline monoclinic, hexagonal, and tetragonal one-dimensional (1D) $LnPO_4$ nanostructures of different aspect ratios through kinetically controlled hydrothermal growth processes is also demonstrated. It is shown that the tendency for anisotropic growth can be enhanced simply by modifying the chemical potential of species in the hydrothermal environment through the use of carefully selected chelating ligands. A systematic study of the photoluminescence in a series of Eu^{3+}-doped lanthanide phosphates has shown that the optical properties of these nanophosphors are strongly dependent on their crystal structures and morphologies.

Results and Discussion

Switches of crystal structure and morphology evolution: synthesis and characterization of $LnPO_4{\cdot}nH_2O$ (n = 0–1) (Ln = La→Nd, Sm→Tb) nanowires and $LnPO_4$ (Ln = Dy→Lu, Y) nanoparticles: Hydrothermal treatment of the amorphous particle dispersions generated by direct precipitation of Ln^{3+} (Ln = La–Nd, Sm–Lu, Y) and PO_4^{3-} under identical conditions (180 °C, 2 days, pH 1–2) led to the formation of lanthanide orthophosphates of three different crystal structure types (see Table 1).

Table 1. Crystal structures and morphologies of lanthanide phosphates obtained under identical synthetic conditions (180 °C, 2 days, pH 1–2).

Crystal structure	Monoclinic			Hexagonal						Tetragonal
Ln^{3+}	La^{3+}	Ce^{3+}	Nd^{3+}	Pr^{3+}	Sm^{3+}	Eu^{3+}	Gd^{3+}	Tb^{3+}	Y^{3+}/La^{3+}	Y^{3+}, Dy^{3+}–Lu^{3+}
morphology[a]	NW	NW	NR	NR	NW	NR	NW	NR	NR	NP

[a] NW = nanowire, NR = nanorods, NP = nanoparticles.

For the larger lanthanide ions (Ln = La, Ce, Nd), the corresponding phosphates crystallized in the monoclinic structure of monazite. The X-ray diffraction pattern of $LaPO_4$ is shown in Figure 1. All reflection peaks can be readily indexed as arising from a pure monoclinic phase (JCPDS 84–0600, space group $P2_1/n$ (no. 14)) with lattice constants a = 6.825, b = 7.057, c = 6.482 nm, and β = 103.210°. Similar XRD patterns of a monoclinic phase were also observed for $CePO_4$ (JCPDS 83–0652) and $NdPO_4$ (JCPDS 83–0654).

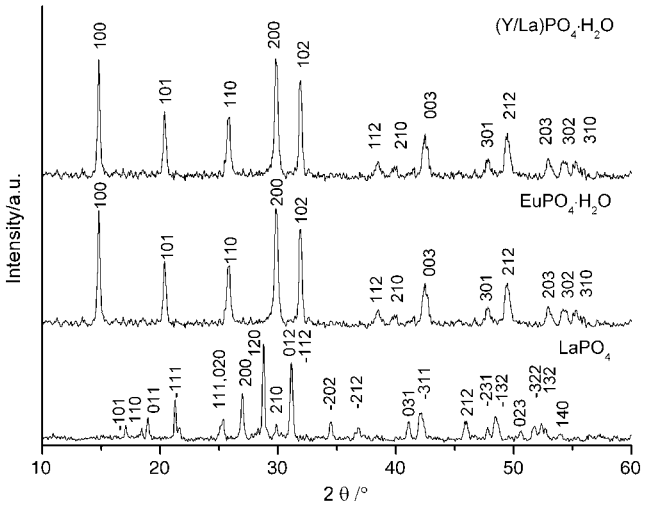

Figure 1. XRD patterns of monoclinic $LaPO_4$ and hexagonal $EuPO_4{\cdot}H_2O$ and (Y/La)$PO_4{\cdot}H_2O$ nanowires/nanorods.

The XRD pattern of the corresponding phosphate of Eu^{3+} indicates that it adopts a different crystal structure. All the reflection peaks can be indexed to the pure hexagonal phase of $EuPO_4{\cdot}H_2O$ (space group $P3_121$ (no. 152)) with lattice constants a = 6.91 and c = 6.34 nm (JCPDS 20–1044). Similar XRD patterns are also observed for phosphates of other lanthanide ions from the middle part of the lanthanide series (Ln = Pr, Sm, Eu, Gd, Tb), all of which were obtained as phosphate hydrates and were found to exhibit hexagonal structures.

Hexagonal orthophosphates of La^{3+} to Dy^{3+} (space group $P3_121$) have also been reported by Fang et al.[27] The peak positions and relative peak intensities in the XRD patterns of these products are almost identical to those given in Figure 1. Interestingly, however, the authors ascribed these hexagonal structures not to lanthanide phosphate hydrates $LnPO_4{\cdot}nH_2O$, but to anhydrous $LnPO_4$. Although the existence of hexagonal structures of completely anhydrous $LaPO_4$, $CePO_4$, and $NdPO_4$ is unambiguously demonstrated by the JCPDS data (nos. 04–0635, 04–0632, 04–0644), we failed to find corresponding JCPDS cards or related literature for other anhydrous hexagonal $LnPO_4$. For Ln = La, Ce, and Nd, both monoclinic and hexagonal $LnPO_4$ phases exist. For Ln = Pr, Sm, Eu, Gd, and Tb, however, only monoclinic $LnPO_4$ structures are found; the hexagonal phase only exists for the corresponding phosphate hydrates. This is consistent with the results summarized by Wickleder in his review of lanthanide phosphates.[30] Thermogravimetric analysis further confirmed the hydrated nature of the derived

hexagonal lanthanide phosphates. Figure 2 shows a typical TGA curve for these samples. A sudden drop in the weight of the sample at around 150 °C clearly indicates a rapid loss of water molecules from the crystal lattice. Thus, the as-synthesized hexagonal nanostructures, as well as those reported by Fang et al., are believed to be lanthanide phosphate hydrates.

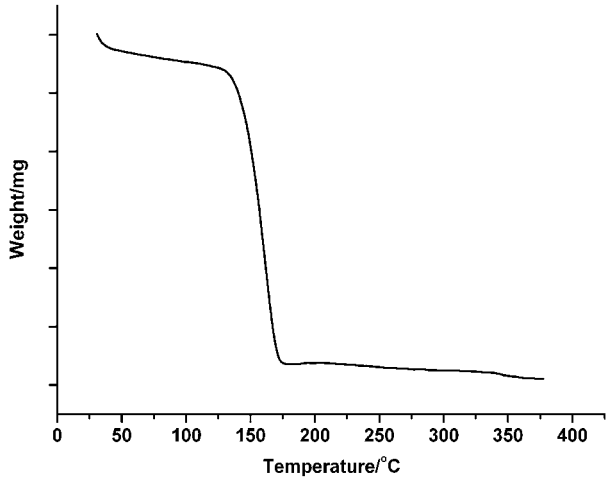

Figure 2. TGA curve of $GdPO_4 \cdot H_2O$ nanowires.

With smaller Ln^{3+} ions (Ln = Dy, Ho, Er, Tm, Yb, Lu, Y), the obtained orthophosphates crystallized in the tetragonal structure of xenotime. All reflection peaks of the seven isostructural $LnPO_4$ can be readily indexed as arising from a pure tetragonal phase (space group $I4_1/amd$). It can be seen from Figure 3 that the 2θ values of the XRD peaks gradually increase on going from $DyPO_4$ to $LuPO_4$, indicating the gradual shrinkage of lattice constants and cell volumes.

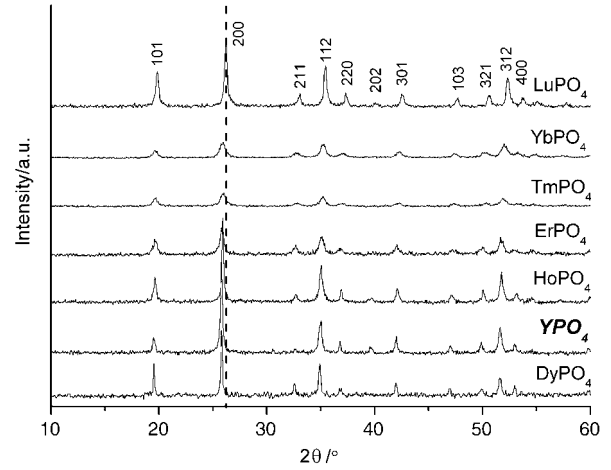

Figure 3. XRD patterns of tetragonal $LnPO_4$ nanoparticles.

This shrinkage of the lattice constants with increasing atomic number, which is also observed for monoclinic and hexagonal phases of lanthanide phosphates, is believed to be caused by the contraction of the ionic radii of Ln^{3+}. This conclusion is confirmed by comparing the lattice constants and ionic radius of tetragonal YPO_4 with the corresponding parameters for tetragonal $LnPO_4$. Table 2 lists the effective ionic radii of Ln^{3+} and Y^{3+} for a coordination number of 8 and the measured lattice constants a and c of the corresponding tetragonal phosphates. It can be seen that although Y^{3+} is much lighter in weight than the heavy lanthanide ions like Dy^{3+} and Ho^{3+}, its lattice parameters are very close to those of the heavier cations and in fact lie between those of Dy^{3+} and Ho^{3+}, which correlates well with the relative effective ionic radii.

It is very interesting that the lanthanide phosphates derived under identical synthesis conditions adopted three different crystal structures. Although the exact reason for this phenomenon is not yet clearly known, the switches of crystal structure seem to be closely related to the gradual contraction of the Ln^{3+} radius. Generally, for larger Ln^{3+}, a monoclinic structure is preferred. For Ln^{3+} of intermediate size, a partly hydrated hexagonal structure is more favorable. For the smaller heavy Ln^{3+} ions, a tetragonal phase is adopted.

Table 2. Effective ionic radii of Dy^{3+}–Lu^{3+}, Y^{3+} and the lattice constants of (Dy–Lu,Y)PO_4.

		Dy^{3+}	**Y^{3+}**	Ho^{3+}	Er^{3+}	Tm^{3+}	Yb^{3+}	Lu^{3+}
effective ionic radius [Å][a]	1.03	**1.015**	1.02	1.00	0.99	0.98	0.97	
Lattice constants	a [nm]	6.91	**6.8947**	6.882	6.86	6.82	6.817	6.792
	c [nm]	6.04	**6.0276**	6.025	6.003	5.97	5.972	5.954

[a] For a coordination number (CN) of 8 (*CRC Handbook of Chemistry and Physics*, 83rd edition).

Except in the monoclinic phase, where the coordination number of Ln^{3+} is 9, Ln^{3+} in both the hexagonal and tetragonal phases is eight-coordinate, because as the radius of the Ln^{3+} decreases, the accommodation of an extra coordinating O atom becomes increasingly difficult. The correlation between the Ln^{3+} radii and crystal structures of $LnPO_4$ made us wonder what would happen if a larger Ln^{3+}, which originally crystallized in monoclinic phase, and a smaller Ln^{3+}, from which tetragonal structures were obtained, were to be co-precipitated by PO_4^{3-}. For example, with La^{3+} and Y^{3+} mixed in a 1:1 ratio, the final product might conceivably be a mixture of the monoclinic $LaPO_4$ and tetragonal YPO_4. However, it may also be a mixed phosphate (La/Y)$PO_4 \cdot n H_2O$ ($n = 0$), and since the average cation radius in this system is close to that of a mid-range Ln^{3+} ion, this mixed phosphate could very possibly adopt a hexagonal structure. Interestingly, the experimental results proved that the derived mixed phosphate of La^{3+} and Y^{3+} (1:1) did indeed crystallize in the hexagonal phase, as demonstrated by the XRD pattern (Figure 1). Moreover, it was also shown

to be a phosphate hydrate like the hexagonal $LnPO_4 \cdot n H_2O$ derived from medium-sized Ln^{3+}. This successful demonstration may assist us in understanding the fundamentals of phase evolution of lanthanide phosphates, which are closely related to the varying effective cation radii.

The size and morphology of the as-synthesized lanthanide phosphates were further examined by transmission electron microscopy (TEM). As shown in Figure 4A, a typical TEM image of $LaPO_4$ nanowires displays uniform morphologies with diameters of 20–30 nm and lengths up to 1 μm. The electron diffraction pattern (Figure 4B, inset) taken from a single $LaPO_4$ nanowire reveals the single-crystalline nature of the sample. It can be indexed as monoclinic $LaPO_4$, consistent with the XRD results presented above. The preferred growth direction of the monazite-type nanowires is along the *c* axis [001]. A high-resolution TEM (HRTEM) image (Figure 4B) shows that the nanowire is structurally uniform with good crystallinity. Figures 4C and D show TEM images of monoclinic $CePO_4$ and $NdPO_4$ crystallized in nanowires with aspect ratios of about 50:1 and about 20:1, respectively.

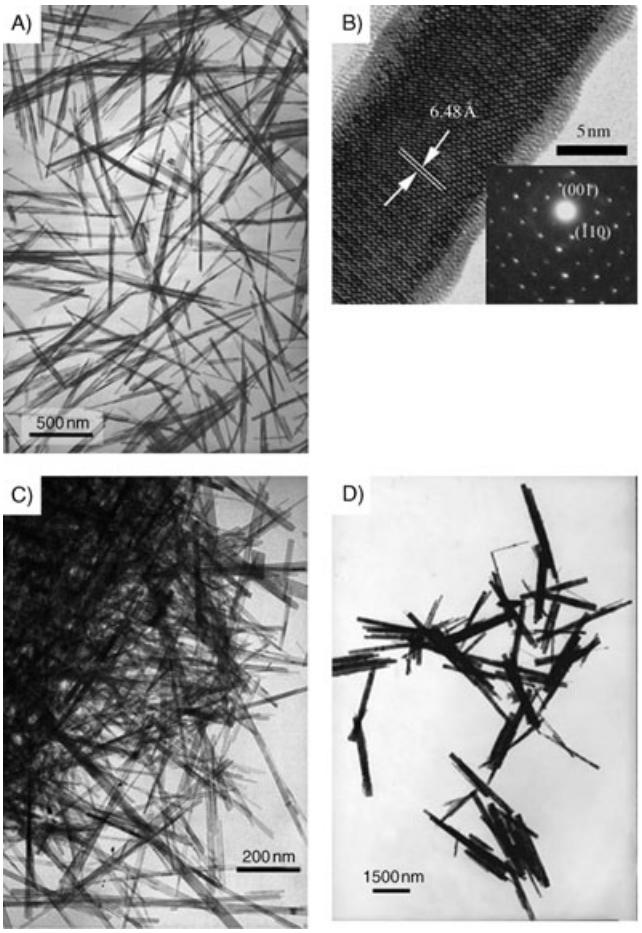

Figure 4. A) TEM image of $LaPO_4$ nanowires; B) HRTEM image and EDAX pattern of a single $LaPO_4$ nanowire; C) TEM image of $CePO_4$ nanowires; D) TEM image of $NdPO_4$ nanowires.

Figure 5 shows typical TEM images of hexagonal $LnPO_4 \cdot nH_2O$. It can be seen that all these products display a uniform rodlike morphology with a length in the range 0.3–3 μm and a width in the range 10–100 nm. It is noteworthy that the $GdPO_4 \cdot H_2O$ nanowires shown in Figure 5E have a very large aspect ratio of ~100. The selected-area electron-diffraction (SAED) pattern shown in Figure 5F suggests that the $GdPO_4 \cdot H_2O$ nanowire grows along the *c* axis [001]. The mixed phosphate $(La/Y)PO_4 \cdot H_2O$ also has a rodlike morphology, as shown in Figure 5G, and the SAED pattern taken from a single nanorod (Figure 5H) again suggests that growth occurs along the *c* axis [001].

Under the same synthetic conditions, the tetragonal $LnPO_4$ (Ln = Dy→Lu, Y) crystals exhibited sphere-like morphology. Figure 6 shows typical TEM images of the obtained tetragonal structured $DyPO_4$ ($Dy^{3+} \rightarrow 4f^9$), $ErPO_4$ ($Er^{3+} \rightarrow 4f^{11}$), and $LuPO_4$ ($Lu^{3+} \rightarrow 4f^{14}$) nanoparticles. No 1D morphology could be observed for these $(Dy \rightarrow Lu, Y)PO_4$ samples.

Hydrothermal methods have been shown to be an effective synthetic means of preparing oriented nanostructures such as nanowires, nanorods, and nanotubes.[31–33] In contrast to synthetic strategies such as the vapor–liquid–solid (VLS) or template-confined methods, the solution-based hydrothermal method adopted here is neither controlled by a catalyst serving as the energetically favorable site for the absorption of reactant molecules (VLS), nor is it guided by templates, surfactants or polymers (template-confined). Thus, it is reasonable to believe that the morphology evolution of the various lanthanide phosphates derived under identical synthetic conditions is closely related to their inherent crystal structures. $LnPO_4 \cdot n H_2O$ (Ln = Pr, Sm, Eu, Gd, Tb) was fabricated in a hexagonal phase similar to that of ZnO[4] and $Ln(OH)_3$,[21] which has been widely recognized as a highly anisotropic structure. Similarly, the monoclinic structure adopted by $LnPO_4$ (Ln = La, Ce, Nd) has also been demonstrated to be highly anisotropic and to aid the formation of various 1D nanostructures in a template-free solution environment.[28,31,34] On the contrary, those phosphates with the smaller metal ion centers are obtained in tetragonal structures, which are less anisotropic and show a reduced tendency to grow along a certain direction. Consequently, the heavier lanthanide phosphates are obtained in the form of nanoparticles under the synthetic conditions.

Controlled synthesis and formation mechanism of 1D tetragonal, monoclinic, and hexagonal $LnPO_4$ nanostructures: Fang et al.[27] and Zhang et al.[28] have also observed the morphology evolution of $LnPO_4$ with different crystal structures, and they both mentioned that no 1D nanostructures of the tetragonal heavy lanthanide phosphates are formed spontaneously under hydrothermal conditions, in contrast to their monoclinic or hexagonal counterparts. Fang et al. studied the structure of the tetragonal $LnPO_4$ and concluded that since it lacks the infinite chain structure of hexagonal $LnPO_4$, it is isotropic in nature and so does not have any preferred growth direction.

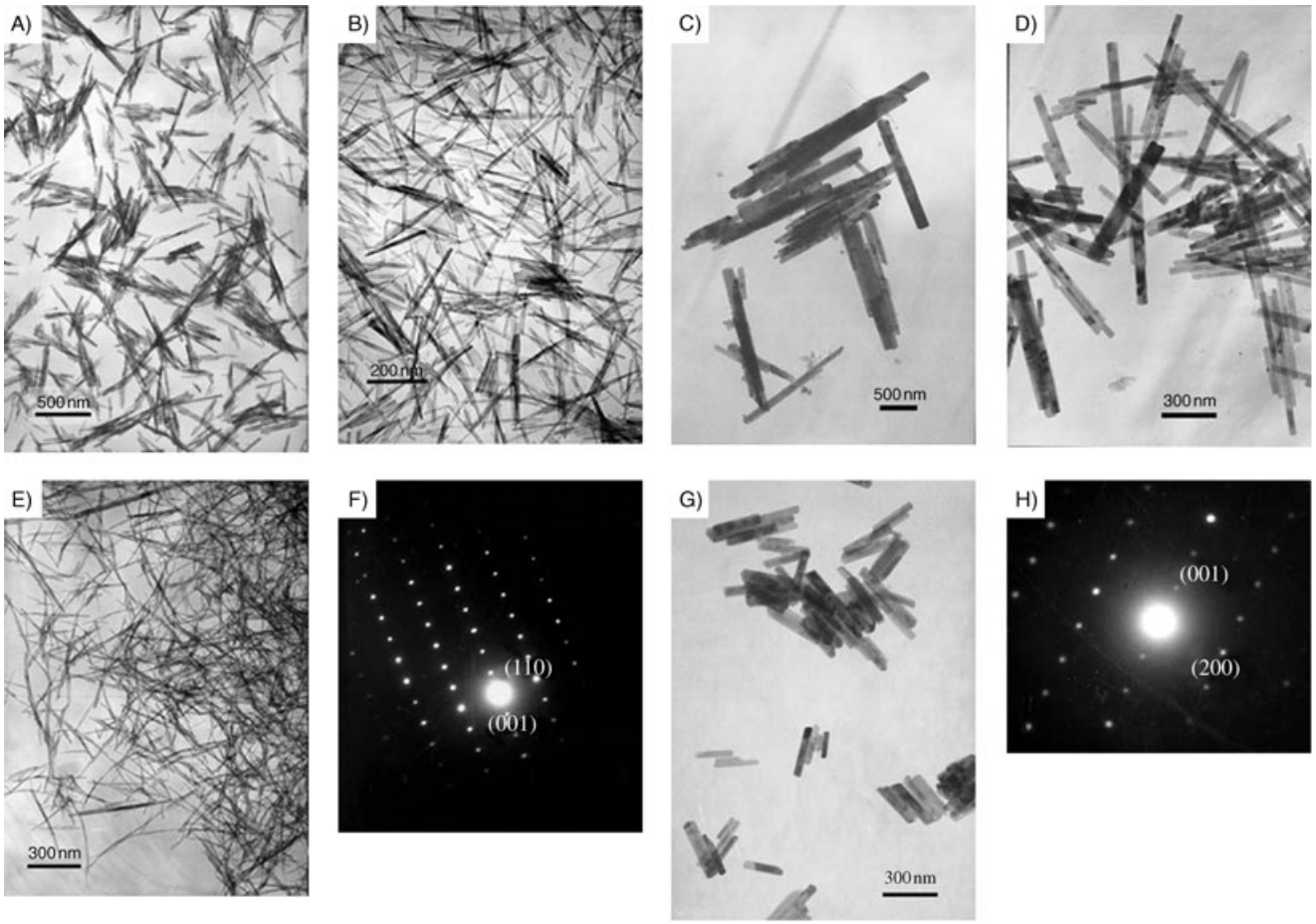

Figure 5. A) TEM image of $PrPO_4{\cdot}H_2O$ nanorods; B) TEM image of $SmPO_4{\cdot}0.5H_2O$ nanowires; C) TEM image of $EuPO_4{\cdot}H_2O$ nanorods; D) TEM image of $TbPO_4{\cdot}H_2O$ nanorods; E) TEM image of $GdPO_4{\cdot}H_2O$ nanowires; F) EDAX pattern of a single $GdPO_4{\cdot}H_2O$ nanowire; G) TEM image of (Y/La)$PO_4{\cdot}H_2O$ nanorods; H) EDAX pattern of a single (Y/La)$PO_4{\cdot}H_2O$ nanorod.

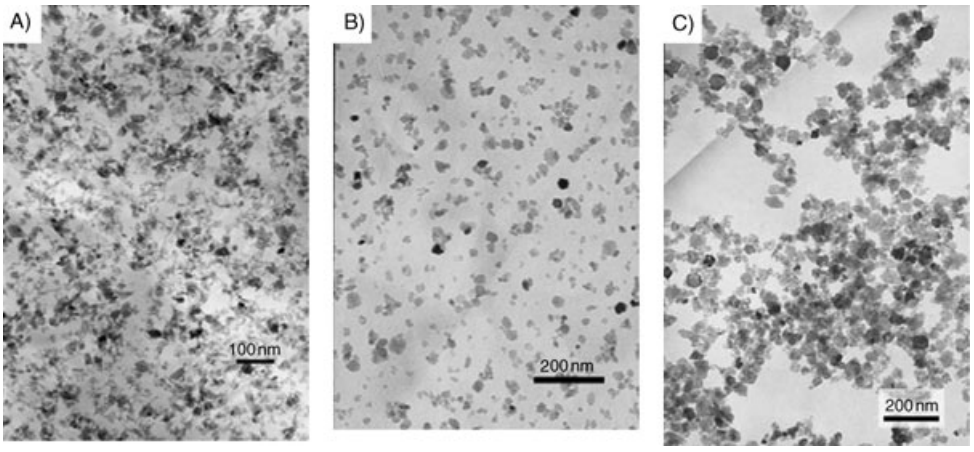

Figure 6. A) TEM image of $DyPO_4$ nanoparticles; B) TEM image of $ErPO_4$ nanoparticles; C) TEM image of $LuPO_4$ nanoparticles.

However, a more careful examination of the crystal structure of the tetragonal $LnPO_4$ suggested otherwise. Views of the molecular arrangement of tetragonal $HoPO_4$ along the *a* and *c* axes are presented in Figure 7A and Figure 7B, respectively.[35] Since the tetragonal heavy lanthanide phosphates and YPO_4 are isostructural, their structural features are identical. It can be seen that the molecular packing arrangement of tetragonal $HoPO_4$ is neither a one-dimensional infinite chain structure nor a two-dimensional lamellar structure, but a three-dimensional network structure, which, in the view of Fang et al., is not subject to anisotropic growth. However, the anisotropic growth of nanocrystals has been shown to be strongly dependent on relative chemical potentials, as highlighted by Peng et al.[14,15] According to Gibbs–Thompson theory, the relative chemical potential of a crystal is simply proportional to its surface–atom ratio, determined by the average number of dangling bonds per atom over the

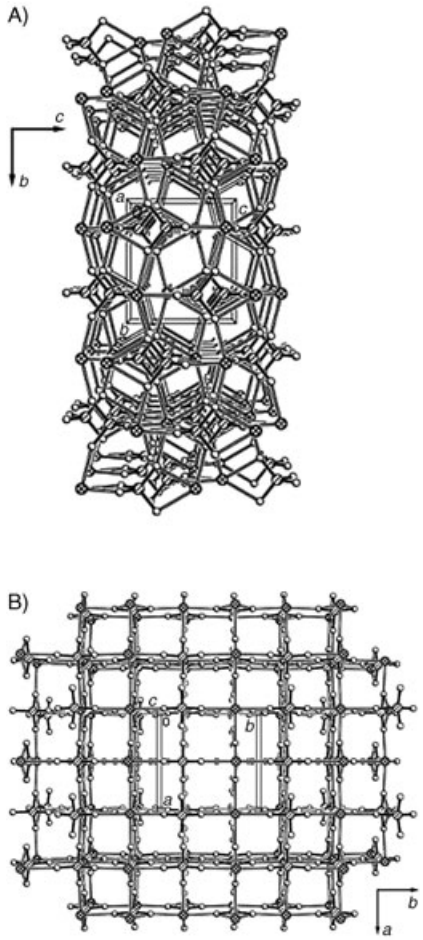

Figure 7. A) Perspective view along the *a* axis of the molecular packing of $HoPO_4$; B) perspective view along the *c* axis of the molecular packing of $HoPO_4$ (dashed circle = P, open circle = O, crossed circle = Ho).

entire crystal.[33] From Figure 7A and B, we can see that for each PO_4^{3-} tetrahedron attached along the ⟨100⟩ direction, or the *a* axis, two O atoms are used to form Ho–O bonds along the *a* axis, while the other two O atoms form Ho–O bonds along the *b* and *c* axes, respectively, without contributing to the growth on the (100) facet. Since *a* and *b* are equivalent axes in tetragonal systems, the packing fashion of PO_4^{3-} tetrahedra along the two axes is much the same. From Figure 7A, we can also see that for each PO_4^{3-} tetrahedron attached to the (001) facet, or the *c* axis, three O atoms are used to form Ho–O bonds along the *c* axis, while the other O atom forms a Ho–O bond along the *a* axis. Furthermore, it is clear from Figure 7B that when PO_4^{3-} is attached to the (110) facet, all four O atoms of the PO_4^{3-} tetrahedron bond to the Ho atom along the ⟨110⟩ direction, contributing non-specifically to the growth along this particular direction. It is clear that the (110) facet bears more dangling bonds and that growth along the ⟨110⟩ direction releases more energy, thus making the (110) facet of higher chemical potential than the (100), (010), and (001) facets.

This special feature of the (110) facet of this tetragonal structure may shed some light on the anisotropic nature of heavy lanthanide phosphates, although the tendency for anisotropic growth of these tetragonal $LnPO_4$ may not be as strong as that of their monoclinic and hexagonal counterparts, as indicated by the experimental results. However, under suitable synthetic conditions, the intrinsic anisotropic feature of tetragonal $LnPO_4$ may be magnified, leading to the formation of 1D nanostructures. Peng et al.[14] have shown that one-dimensional growth only occurs if the chemical potential of the monomers in solution is much higher than the highest chemical potential of the atoms on the surface of the nanocrystals. This concept has been extensively demonstrated in hydrothermal syntheses of various 1D nanostructures.[21,27,28,33] It is also reasonable to assume that oriented growth of the tetragonal $LnPO_4$ can be ensured by modifying the composition of the solution such that the chemical potential of the monomer is maximized.

Figure 8 shows TEM images of the YPO_4 nanocrystals obtained when Y^{3+} was complexed with EDTA at various concentrations prior to precipitation with PO_4^{3-}. It can clearly be seen that on increasing the amount of EDTA present in the original hydrothermal environment, the morphology of the YPO_4 nanocrystals varies from one of nanoparticles to one of nanorods, reflecting increased oriented growth. Similar tendencies were also observed for other tetragonal heavy $LnPO_4$ nanocrystals; Figure 9 shows TEM images of $HoPO_4$ nanowires and $DyPO_4$ and $ErPO_4$ nanorods obtained in the

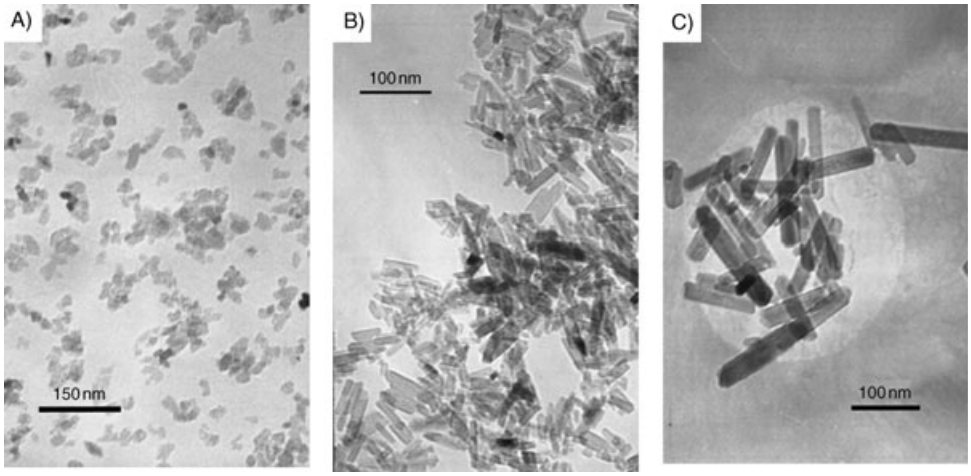

Figure 8. A) TEM image of YPO_4 nanoparticles (180 °C, 0.1 g EDTA); B) TEM image of YPO_4 nanoparticles (180 °C, 0.3 g EDTA); C) TEM image of YPO_4 nanoparticles (180 °C, 0.5 g EDTA).

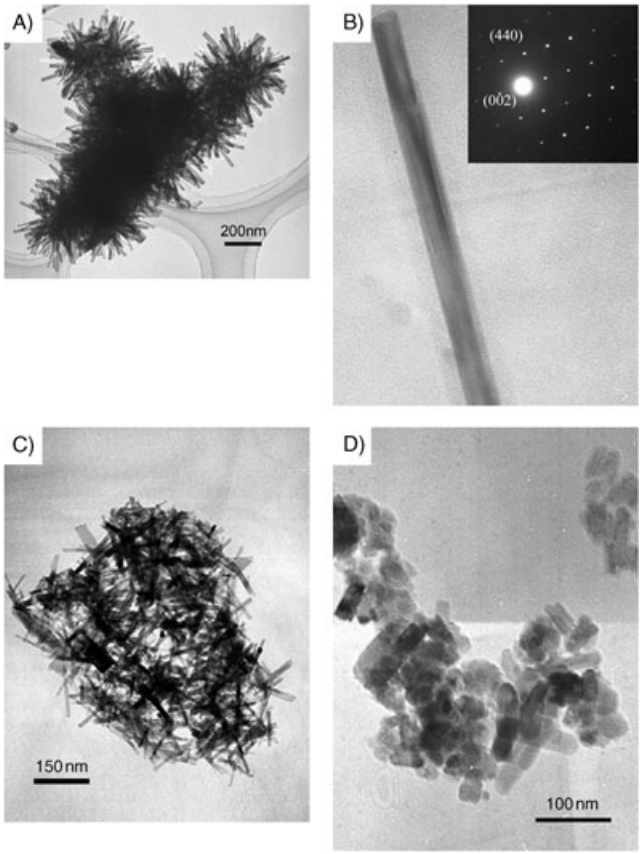

Figure 9. A) TEM image of $HoPO_4$ nanowires (180 °C, EDTA); B) a single $HoPO_4$ nanowire and its EDAX pattern (180 °C, EDTA); C) TEM image of $DyPO_4$ nanorods (180 °C, EDTA); D) TEM image of $ErPO_4$ nanorods (180 °C, EDTA).

presence of EDTA, indicating the anisotropic nature of this type of crystal structure. The $HoPO_4$ nanowires are 10–15 nm in width and more than 200 nm in length, thus giving them an aspect ratio of over 10, and are self-aggregated into urchin-like bundles. The diameter of $DyPO_4$ nanowires is also 10–15 nm, which is similar to that of the corresponding nanoparticles obtained without EDTA. This consistency of diameters is also observed for $HoPO_4$, $ErPO_4$, and YPO_4. The aspect ratio of $ErPO_4$ nanorods is about 2–3, which is relatively small compared to the values for other tetragonal $LnPO_4$ 1D nanocrystals; nonetheless, the difference between these rods and the nanoparticles derived without EDTA (Figure 6B) is evident. Neither the obvious self-aggregation growth mechanism involving mostly linearly oriented particle aggregation,[36] nor the spontaneous organization of small nanoparticles into greatly elongated nanorods/nanowires,[37] was observed for these tetragonal $LnPO_4$ nanowires/nanorods.

Electron diffraction patterns (Figure 9B) taken from a single $HoPO_4$ nanowire also demonstrated unambiguously the single-crystalline nature of the sample; it can be readily indexed as tetragonal $HoPO_4$, in good agreement with its XRD data. The preferred growth direction of the zircon-type nanowires was determined to be along the ⟨110⟩ direction, consistent with the preferred growth direction indicated by the structural analysis described above.

The experimental results have shown that the presence of EDTA is an important factor in guiding the anisotropic growth of tetragonal lanthanide phosphates. Although a quantitative thermodynamic prediction of the crystallization in the nanometer regime for this synthetic system is still very difficult and requires extensive research,[38] the function of EDTA can be understood by analyzing the growing environments with and without complexation by this ligand. It can be seen that the two growing environments are very different in nature.

Without EDTA, the system undergoes a typical hydrothermally induced process. Initially, direct mixing of the two solutions yields a supersaturated medium and leads to the formation of a large number of amorphous fine particles, and these act as precursors for the synthesis of crystalline $LnPO_4$. Thus, tiny crystalline nuclei are formed in a supersaturated medium at elevated temperatures under hydrothermal conditions, and this is followed by crystal growth. The larger particles grow at the expense of the small ones due to their different solubilities, in accordance with the well-known Gibbs–Thomson law. However, when the Ln^{3+} is treated with a high concentration of EDTA, no noticeable precipitation occurs upon the addition of PO_4^{3-} at room temperature and the system remains homogeneous prior to hydrothermal treatment. The Ln^{3+} present in the solution is in the form of the Ln^{3+}-EDTA complex and PO_4^{3-} exists as the free anion. As the temperature is increased, the Ln^{3+}-EDTA complex gradually dissociates, releasing the Ln^{3+} into the solution. The crystalline nuclei are formed slowly at this stage, resulting in a relatively small concentration of nuclei compared to that obtained with the EDTA-free system. In the ensuing crystal growth stage, both monomers have high chemical potential since most PO_4^{3-} ions are free in the solution and Ln^{3+} ions are continuously supplied at a convenient rate from the thermal decomposition of the Ln^{3+}-EDTA complex, which serves as an Ln^{3+} reservoir. The high chemical potentials of both PO_4^{3-} and Ln^{3+} in the solution provide more favorable conditions for the anisotropic growth of tetragonal $LnPO_4$.

It should be noted that increasing the concentration of either PO_4^{3-} or Ln^{3+} alone did not significantly aid the anisotropic growth of tetragonal $LnPO_4$. Control experiments showed that when the $[Ln^{3+}]/[PO_4^{3-}]$ ratio was adjusted to 1:5 or 5:1, no sign of oriented growth was observed. The growth of the $LnPO_4$ nanocrystals in these systems still conforms to the hydrothermally induced process, and although one of the monomers has a higher chemical potential, the other is quickly consumed from the bulk solution, its concentration being strictly limited by the K_{sp} of the corresponding $LnPO_4$. Later, the growth rate along the ⟨110⟩ direction is slowed, even though it had the highest chemical potential.

Experimental results have shown that the addition of EDTA to this hydrothermal system can accelerate the anisotropic growth of tetragonal $LnPO_4$ along a preferred direc-

tion. However, this effect of EDTA is not limited to the specific case of tetragonal $LnPO_4$. Experimental results have also indicated that the tendency for oriented growth of monoclinic $LnPO_4$ and hexagonal $LnPO_4{\cdot}nH_2O$ can also be enhanced by adding EDTA at the initial stage. Figures 10A and B show TEM images of monoclinic $LaPO_4$ obtained at pH 1 and 10, respectively. It can be seen that the aspect ratio of the $LaPO_4$ nanowires is greatly reduced in the alkaline environment, mainly because the La^{3+} ions are prone to precipitation as the hydroxide at higher pH values and their chemical potential is thereby reduced. However, when EDTA is added to chelate the La^{3+} at the beginning, the precipitation of these cations by OH^- can be suppressed even at higher pH values, and their chemical potential is thereby increased, promoting the anisotropic growth. As a result, the aspect ratio of $LaPO_4$ nanorods obtained in the presence of EDTA at pH 10 was higher (Figure 10C) and the nanorods were also found to be more uniform in morphology. TEM images of hexagonal $GdPO_4{\cdot}H_2O$ (Figure 10D, E, and F) obtained under different conditions (pH 1, pH 10 without EDTA, and pH 10 with EDTA, respectively) indicate that the presence of EDTA can also promote oriented growth of the hexagonal structure in alkaline solution.

Control experiments were carried out to screen for the most effective chelating agents in guiding the formation of tetragonal $LnPO_4$ nanowires/nanorods. Commonly used ligands such as diethylamine, citric acid, and oxalic acid, among others, were employed in the same approach. Although diethylamine and other NH_2-bearing ligands have proved to be very effective in guiding the growth of other 1D nanostructures,[39] adding these alkaline ligands to the present system results in the mother liquor having a very high pH value, conditions under which bulk precipitation of $Ln(OH)_3$ is inevitable. On the other hand, it seems that common acidic ligands such as oxalic acid, which rely on the chelating effect of -COOH or $-COO^-$, cannot form water-soluble complexes with Ln^{3+} ions. On the contrary, the Ln^{3+}-EDTA complex is stable and water-soluble over a much wider pH range, and thus is best suited for the specific requirements of this system.

Optical properties of Eu^{3+}-doped $LnPO_4$ of different crystal types: Lanthanide phosphates have been shown to be a useful host lattice for other lanthanide ions, producing phosphors emitting a variety of colors.[23] Although series of lanthanide phosphate nanowires/nanorods have been successfully synthesized by several groups, the optical properties of lanthanide-doped $LnPO_4$ nanowires/nanorods have only been studied in very limited doping systems.[25,27] A systematic study of the optical behavior of Ln^{3+}-doped $LnPO_4$ nanowires/nanorods is still lacking. In the course of our work, we prepared a series of Ln^{3+}-doped $LnPO_4$ nanowires/nanorods of different aspect ratios and different crystal structures, and the evolution of the spectral behavior with morphology and crystal structure was systematically studied. Eu^{3+} is adopted as a doping ion to probe structural differences because its emission spectrum is very sensitive to the local chemical environment. It should be noted that the doped samples were prepared by a similar hydrothermal

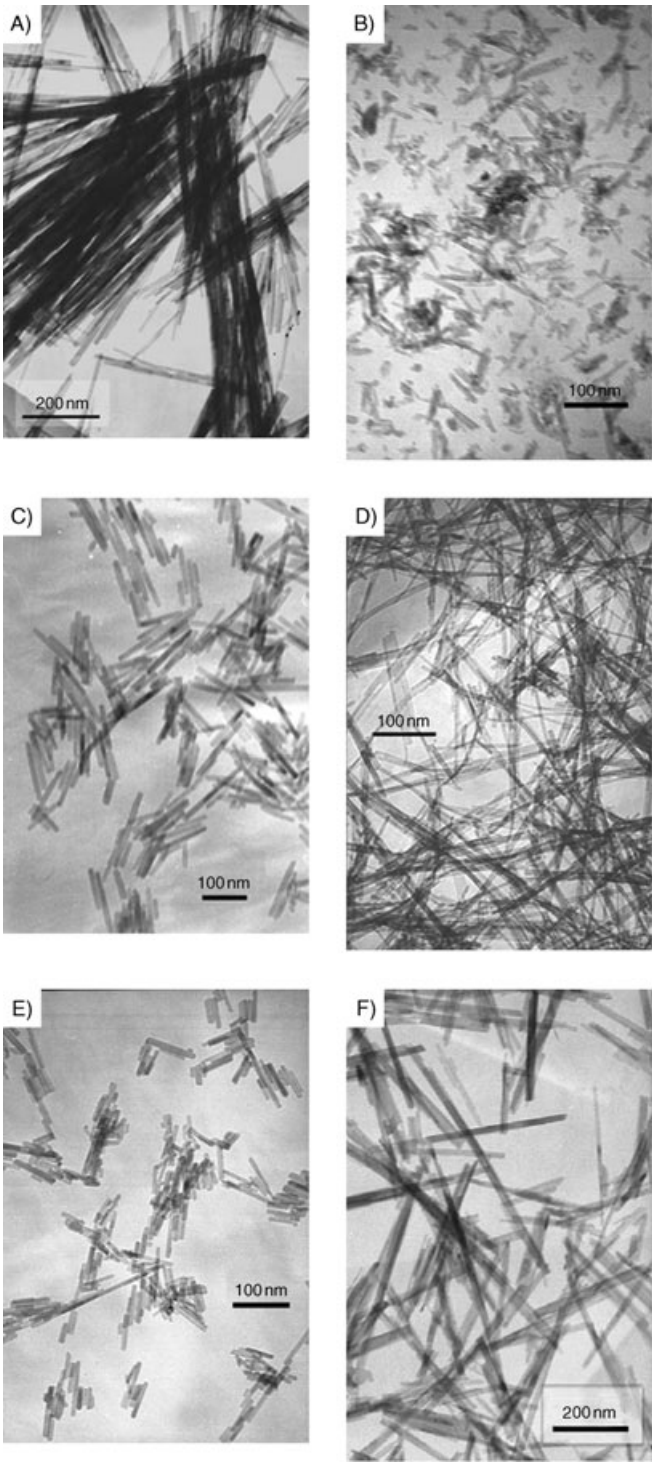

Figure 10. TEM images of A) $LaPO_4$ nanowires (180 °C, pH 1, without EDTA), B) $LaPO_4$ nanorods (180 °C, pH 10, without EDTA), C) $LaPO_4$ nanowires (180 °C, pH 10, with EDTA), D) $GdPO_4{\cdot}H_2O$ nanowires (180 °C, pH 1, without EDTA), E) $GdPO_4{\cdot}H_2O$ nanorods (180 °C, pH 10, without EDTA), and F) $GdPO_4{\cdot}H_2O$ nanowires (180 °C, pH 10, with EDTA).

treatment as the undoped samples without high-temperature annealing, and that the doping alters neither the crystal structure nor the morphology of the host material.

Room-temperature excitation and emission spectra of $LaPO_4$:Eu(10%) nanowires and nanorods are presented in Figure 11A and B, respectively (the doping concentration

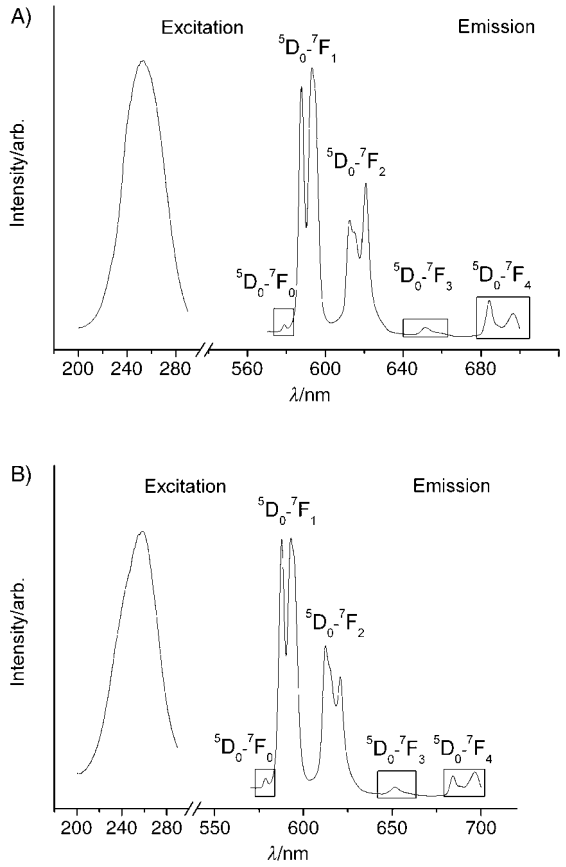

Figure 11. Excitation and emission spectra of monoclinic A) $LaPO_4$:Eu(10%) nanowires obtained at 180°C, pH 1; B) $LaPO_4$:Eu(10%) nanorods, obtained at 180°C, pH 10.

was experimentally determined to be 9.944% by XRF analysis). The $LaPO_4$:Eu nanowires were derived from hydrothermal treatment at 180°C starting at pH 1, while the $LaPO_4$:Eu nanorods were prepared at 180°C starting at pH 10. Both products adopted a monoclinic crystal structure.

In the excitation spectrum of monazite $LaPO_4$:Eu nanowires (Figure 11A, left), the broad band centered at 253 nm is attributed to a charge-transfer (CT) transition, which occurs by electron delocalization from the filled 2p shell of the O^{2-} to the partially filled 4f shell of Eu^{3+}. The position of the charge-transfer band (CTB) observed for these $LaPO_4$:Eu nanowires is the same as in the case of bulk $LaPO_4$:Eu (253 nm),[40] indicating a similar local environment of the Eu^{3+} ions in the host lattices. However, a small shift of the CTB could be observed for the $LaPO_4$:Eu nanorods (Figure 11B, left), with the maximum appearing at 259 nm. Previous studies of the CTB of Eu^{3+} in different host lattices[41] have indicated that its position depends both on the Eu–O bond length and on the coordination environment about Eu^{3+}. It is more or less fixed in a particular crystal field, but it varies as a function of the host lattice. The variation is proportional to the Eu–O distance: the longer the Eu–O bond, the longer the wavelength of the CTB. Hence, the small red shift observed for $LaPO_4$:Eu nanorods indicates that the average Eu–O bond distance is somewhat longer in $LaPO_4$:Eu nanorods than in $LaPO_4$:Eu nanowires or bulk $LaPO_4$:Eu.

Successful doping with europium was evident from the splitting and the intensity pattern of the luminescence lines. The emission spectra of $LaPO_4$:Eu nanocrystals consist of lines mainly located in the red spectral area (from 570 nm to 700 nm). These lines correspond to transitions from the excited $^5D_0$ levels to the ^7F_J (J = 0,1,2,3,4) levels of the $4f^6$ configuration of Eu^{3+}, as marked in Figure 11. The orange-red emission lines at around 590 nm originating from the magnetic dipole transition $^5D_0 \rightarrow {}^7F_1$ are the dominant bands for both $LaPO_4$:Eu nanowires and nanorods. The intensities of different $^5D_0 \rightarrow {}^7F_J$ transitions and the splittings of these emission transitions depend on the local symmetry of the crystal field of the europium ions. In bulk $LaPO_4$ of monazite structure, the main Eu^{3+} site has C_1 symmetry. The splitting of the energy levels has been calculated for this point group, and is in good agreement with the optical transitions actually observed in bulk $LaPO_4$:Eu.[42] For both $LaPO_4$:Eu nanowires and nanorods, the splitting pattern of each $^5D_0 \rightarrow {}^7F_J$ transition is in accord with the spectrum of the bulk material.

It can be seen from the emission spectra (Figure 11A and B, right) that while the transition energies are the same for $LaPO_4$:Eu nanowires and nanorods, the intensity patterns of their luminescence spectra show some small differences. The relative intensities of the lines due to the $^5D_0 \rightarrow {}^7F_2$ transitions are different in the two cases. A similar deviation can be observed for the components of the $^5D_0 \rightarrow {}^7F_1$ and $^5D_0 \rightarrow {}^7F_4$ transitions. This may be related to the occupancy of the main sites and the additional europium sites with slightly distorted geometry and the rate constants for the energy transfer between adjacent sites.[42] However, the exact geometry of the distortion of a lattice site cannot be accurately deduced from the luminescence spectrum, since theories that provide a basis for carrying out quantitatively reliable intensity calculations on the f–f transitions have yet to be developed.[25]

The fluorescence of rare-earth ions mainly originates from electron transitions within the 4f shell. For trivalent Y, La, and Lu ions, however, the 4f shells are either empty or completely filled, with electron configurations of $4d^{10}4f^0$, $3d^{10}4f^0$, and $4d^{10}4f^{14}$, respectively. No f–f transitions are possible, hence the phosphates of these ions are transparent in the visible spectral region and can serve as desirable host lattices for Eu^{3+}. Similarly, trivalent Gd has a half-filled 4f shell and the realization of any f–f transitions would involve the breaking of the stable $4d^{10}4f^7$ configuration. As a result,

the transition energy for f–f transitions of Gd^{3+} is much higher than for other Ln^{3+} with partially filled 4 f shells, and so its corresponding phosphate is also transparent in the visible region and can serve as a host material. Thus, we examined the feasibility of doping the lattices of hexagonal $GdPO_4{\cdot}H_2O$ and $(La/Y)PO_4{\cdot}H_2O$ and of tetragonal YPO_4 and $LuPO_4$ with Eu^{3+} and studied the optical behavior of the resulting materials.

The excitation and emission spectra of $GdPO_4{\cdot}H_2O$:Eu(10%) and $(La/Y)PO_4{\cdot}H_2O$:Eu(10%) are shown in Figure 12A and Figure 12B, respectively. It can be seen that the

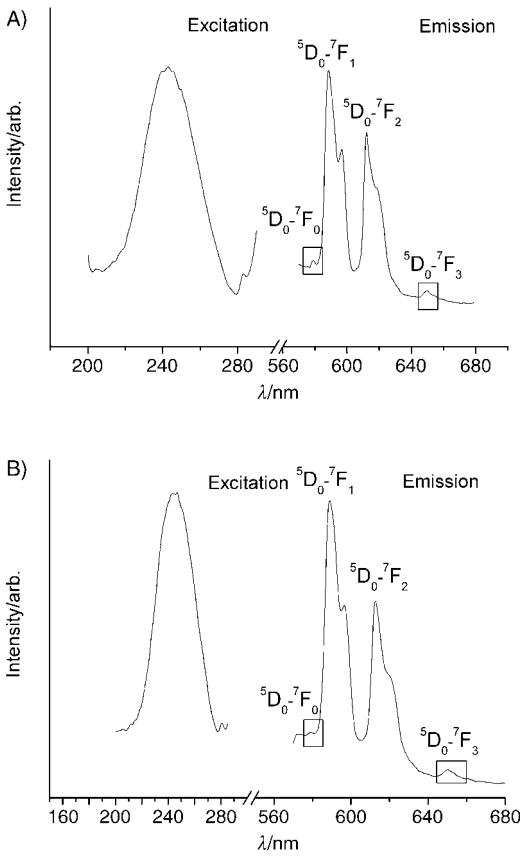

Figure 12. Excitation and emission spectra of hexagonal lanthanide phosphate hydrates: A) $GdPO_4{\cdot}H_2O$:Eu(10%) nanowires obtained at 180°C, pH 1; B) $(Y/La)PO_4{\cdot}H_2O$:Eu(10%) nanorods, obtained at 180°C, pH 1.

position of the CTB of Eu^{3+} in the lattice of hexagonal phosphate hydrates is shifted slightly towards shorter wavelengths compared with its position in monoclinic $LaPO_4$:Eu nanocrystals, being centered at 243 nm for $GdPO_4{\cdot}H_2O$:Eu and at 247 nm for $(La/Y)PO_4{\cdot}H_2O$:Eu. There are corresponding differences in the Eu–O bond lengths. In the lattice of monoclinic $LaPO_4$:Eu, the Ln^{3+} ion is nine-coordinate, and the average length of the nine Ln–O bonds is 2.573 Å.[43] In the lattices of hexagonal lanthanide phosphates, the Ln^{3+} ion is eight-coordinate, and the average length of the eight Ln–O bonds in hexagonal $CePO_4$, which is isostructural with the hexagonal phosphate hydrates,[27] is 2.50 Å.[44] Due to the lanthanide contraction on ascending the series, the cell volume naturally decreases on going from $CePO_4$ (V = 277.75 nm^3) to $GdPO_4{\cdot}H_2O$ (V = 261.23 nm^3); the mixed phosphate $(La/Y)PO_4{\cdot}H_2O$ has a cell volume (V = 269.61 nm^3) intermediate between those of $CePO_4$ and $GdPO_4{\cdot}H_2O$. This indicates that the average Ln–O bond lengths in $GdPO_4{\cdot}H_2O$ and $(La/Y)PO_4{\cdot}H_2O$ are shorter than that in hexagonal $CePO_4$, and even shorter than that in monoclinic $LaPO_4$, although we do not as yet have exact data for the two phosphate hydrates. This also explains the slight red shift of the CTB on going from $(La/Y)PO_4{\cdot}H_2O$:Eu to $GdPO_4{\cdot}H_2O$:Eu.

The emission spectra of the two doped hexagonal systems are very similar, with emission lines in the orange to red spectral range originating from $^5D_0 \rightarrow {}^7F_J$ (J = 0,1,2,3,4) transitions of the $4f^6$ configuration of Eu^{3+}. The close resemblance of the intensity patterns and the splittings of the various $^5D_0 \rightarrow {}^7F_J$ transitions in the two emission spectra is indicative of the similarity of the local symmetry of the crystal field of the Eu^{3+} site in hexagonal $(La/Y)PO_4{\cdot}H_2O$:Eu and $GdPO_4{\cdot}H_2O$:Eu. The 4 f energy levels of Eu^{3+} are hardly affected by the crystal field because of the shielding of the $5s^2$ $5p^6$ electrons. It is for this reason that there is no noticeable shift in the positions of emission peaks compared to the $LaPO_4$:Eu system.

Figure 13A and Figure 13B depict the excitation and emission spectra of tetragonal YPO_4:Eu(10%) and $LuPO_4$:Eu(10%). The positions of the CTB of Eu^{3+} in the lattices of YPO_4:Eu and $LuPO_4$:Eu are 233 nm and 227 nm, respectively, notably blue-shifted in comparison with its position in the monoclinic $LaPO_4$:Eu and in the two doped hexagonal systems. Based on the abovementioned relationship between E_{CT} and the Eu–O distance, it is reasonable to believe that the average Ln–O bond lengths in YPO_4:Eu and $LuPO_4$:Eu are much shorter than those in $LaPO_4$, $(La/Y)PO_4{\cdot}H_2O$, and $GdPO_4{\cdot}H_2O$. This is corroborated by the structural data reported by Milligan et al.[45] The average length of the eight Ln–O bonds is 2.336 Å in YPO_4 and 2.303 Å in $LuPO_4$. Again, the longer Ln–O bonds in YPO_4:Eu account for the slight red shift of the CTB on going from YPO_4:Eu to $LuPO_4$:Eu.

Similar to the doped hexagonal systems discussed above, the two tetragonal phosphates doped with Eu^{3+} also exhibit emission spectra that are practically identical, as shown in Figure 13, indicating a close resemblance of the local symmetry of the Eu^{3+} sites in the two host lattices. It should be noted, however, that unlike for the monoclinic and hexagonal systems, the $^5D_0 \rightarrow {}^7F_0$ transition usually seen at around 580 nm is absent for both YPO_4:Eu and $LuPO_4$:Eu. The reason for this lies in the structural difference between these doped systems, the $^5D_0 \rightarrow {}^7F_0$ transition being very sensitive to the local environment of the Eu^{3+} ion. If the Eu^{3+} ion occupies a site in the crystal lattice that has inversion symmetry, optical transitions between the $^5D_0$ and $^7F_0$ levels (ΔJ = 0, and from J = 0 to J = 0) are strictly forbidden by the parity selection rule. However, if there is no inversion symmetry at the site occupied by the Eu^{3+} ion, that is, when the

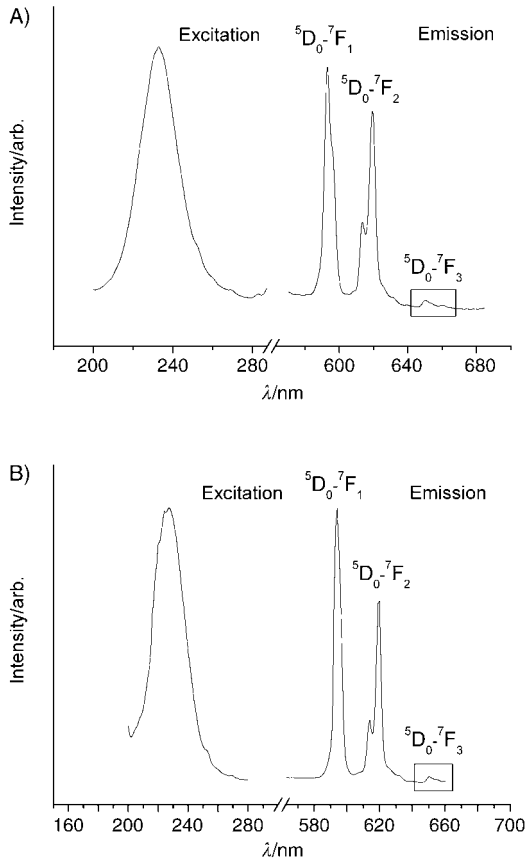

Figure 13. Excitation and emission spectra of tetragonal lanthanide phosphates: A) YPO_4:Eu(10%) nanoparticles obtained at 180°C, pH 1; B) $LuPO_4$:Eu (10%) nanoparticles, obtained at 180°C, pH 1.

Eu^{3+} site has C_s, C_n, or C_{nv} symmetry, the uneven crystal field components can lead to the mixing of opposite parity states into the $4f^n$ configurational levels. The electric dipole transition $^5D_0 \rightarrow {}^7F_0$ is then no longer strictly forbidden and gives rise to weak lines in the spectra. In monoclinic $LaPO_4$:Eu and hexagonal $(La/Y)PO_4 \cdot H_2O$:Eu and $GdPO_4 \cdot H_2O$:Eu, the Eu^{3+} site has C_n or C_{nv} symmetry. The lack of inversion symmetry in these systems allows the appearance of the transition $^5D_0 \rightarrow {}^7F_0$ at 580 nm. On the contrary, the Eu^{3+} in tetragonal YPO_4:Eu and $LuPO_4$:Eu resides at a site with inversion symmetry, most probably S_4 symmetry, so that the $^5D_0 \rightarrow {}^7F_0$ transition is forbidden and the 580 nm line is absent from the emission spectra.

Comparing the PL behavior of all these Eu^{3+}-doped nanostructures, we can see that for host materials of each crystal type both the excitation and emission spectra are very similar. For host materials of two different crystal types, however, not only do the positions of the CTB bands vary significantly, but the splitting and intensity patterns of the emission peaks are also very different. Hence, it is obvious that the optical properties of the Eu^{3+}-doped nanostructures depend greatly on the strength and symmetry of the local crystal fields defined by the crystal structure. Reference spectra of Eu^{3+}-doped bulk lanthanide phosphates are provided in the Supporting Information (Figure S1).

Conclusion

In this research, we have employed the series of lanthanide orthophosphates as a model system to study systematically and in detail the structural and kinetic factors governing the tendency for anisotropic growth and the shape evolution of structures on the nanoscale under hydrothermal conditions. Phase-pure and single-crystalline monoclinic, hexagonal, and tetragonal 1D $LnPO_4$ nanostructures of different aspect ratios have been successfully synthesized in bulk quantities and with high purity by a simple kinetically controlled growth process. Thus, 1D nanostructures of highly anisotropic polymorphs (monoclinic and hexagonal) could be synthesized simply by adjusting the acidity of the stock solution. For tetragonal $LnPO_4$, only irregularly shaped particles could be obtained under similar synthetic conditions. However, based on the intrinsic anisotropy of the crystal structure, the anisotropic growth of tetragonal $LnPO_4$ was realized by varying the chemical potentials of the species in solution through the use of chelating ligands. This successful demonstration may assist us in understanding the fundamentals of the reaction and of nanowire growth mechanisms under hydrothermal conditions. The dynamic processes governing the shape evolution of tetragonal $LnPO_4$ have also been analyzed. This ligand-assisted synthetic strategy for 1D nanomaterials has also been shown to be applicable to other anisotropic crystal structures, such as monoclinic and hexagonal $LnPO_4$. Recently, this synthetic strategy has also been been shown to assist the anisotropic growth of $Ln(OH)_3$ nanocrystals under hydrothermal conditions. It thus seems reasonable to believe that this controlled synthetic strategy and the concept behind it can serve as a general methodology for generating anisotropic nanostructures.

This research has also included an exploration of the key factors that control the evolution of the spectral properties of doped lanthanide phosphate nanocrystals across the series. A systematic study of photoluminescence in various Eu^{3+}-doped lanthanide phosphates was carried out, and the spectral properties of these nanophosphors were shown to depend on their crystal structures and morphologies. This finding indicates the inherent possibility of modifying the optical properties of functional nanocrystals through structural design. These lanthanide phosphates can also be doped with other lanthanide elements, and may be used in fluorescent lamps, in new types of plasma display panels excited by ultraviolet radiation, and as luminescent labels for biomolecules.

Experimental Section

Chemicals: All chemicals were of analytical grade and were used as received without further purification. Deionized water was used through-

out. Ln_2O_3 (Y_2O_3, La_2O_3, Pr_2O_3, Nd_2O_3, Sm_2O_3, Eu_2O_3, Gd_2O_3, Tb_2O_3, Dy_2O_3, Ho_2O_3, Er_2O_3, Tm_2O_3, Yb_2O_3, Lu_2O_3, purity >99.99%), NaH_2PO_4, NaOH, and HNO_3 (A.R.) were all supplied by the Beijing Chemical Reagent Company.

Synthesis of rare-earth phosphate/phosphate hydrate nanowires and nanoparticles: In a typical synthesis, Ln_2O_3 (0.3 g) was dissolved in 10% nitric acid, and then the pH of the solution was rapidly adjusted to a designated value through the addition of 10% NaOH solution. 1 M NaH_2PO_4 solution (20 mL) was then added to the Ln^{3+}-containing solution. A white precipitate of amorphous $LnPO_4$ appeared immediately. After stirring for about 10 min, the precipitate was transferred into a 50-mL autoclave, which was filled with deionized water up to 80% capacity, sealed, and heated at 180 °C for about two days. The system was then allowed to cool to room temperature. The final product was collected by filtration, washed with deionized water to remove any possible ionic remnants, and then dried at 60 °C.

Doped samples were prepared by the same procedure, except that an additional 10% (total molar ratio) Eu_2O_3 was added to the Ln^{3+}-containing solution in the initial step.

In a typical synthesis of tetragonal $LnPO_4$ nanowires/nanorods, Ln_2O_3 (0.3 g) was dissolved in 10% nitric acid, and then EDTA was added to form a clear solution of the Ln^{3+}-EDTA complex. Then the pH of the solution was rapidly adjusted to a designated value through the addition of 10% NaOH solution. 1 M NaH_2PO_4 solution (20 mL) was added to the solution containing Ln^{3+}-EDTA. The solution, which remained clear, was then transferred to a 50-mL autoclave, which was filled with deionized water up to 80% capacity, sealed, and heated at 180 °C for about two days. The system was then allowed to cool to room temperature. The final product was collected by filtration, washed with deionized water to remove any possible ionic remnants, and then dried at 60 °C.

Characterization

Powder X-ray diffraction (XRD): The phase purity of the products was examined by XRD on a Bruker D8 Advance X-ray diffractometer using $Cu_{K\alpha}$ radiation ($\lambda = 1.5418$ Å). The operation voltage and current were kept at 40 kV and 40 mA, respectively. A 2θ range from 10 to 60° was covered in steps of 0.02° with a count time of 2 s.

Transmission electron microscopy (TEM): The crystal size and morphology of the products were examined with a Hitachi Model H-800 transmission electron microscope with a tungsten filament at an accelerating voltage of 200 kV. Samples were prepared by placing a drop of a dilute alcoholic dispersion of nanocrystals on the surface of a copper grid. Electron diffraction and energy-dispersive X-ray analysis were also performed to study the single-crystal nature and elemental compositions of the samples on the H-800 TEM. Structural information on the $LaPO_4$ nanowires was obtained by high-resolution transmission electron microscopy (HRTEM) on a JEOL JEM-2010F transmission electron microscope operated at 200 kV. Electron diffraction studies of the $LaPO_4$ nanowires were also performed on the samples during the HRTEM measurements.

The optical properties of samples were characterized through their photoluminescence (Hitachi F-4500 fluorescence spectrophotometer operated at room temperature with a 150-W continuous-wave xenon lamp).

The doping concentration of the $LaPO_4$:Eu^{3+} sample was characterized by XRF analysis (Shimadzu XRF-1700 sequential X-ray fluorescence spectrometer).

Acknowledgements

This work was supported by the NSFC (50372030, 20025102, 20151001), the Foundation for the Author of National Excellent Doctoral Dissertation of P. R. China, and the State Key Project of Fundamental Research for Nanomaterials and Nanostructures (2003CB716901).

[1] See, for example: A special issue on nanoscale materials: *Acc. Chem. Res.* **1999**, *32*, 387–454.
[2] S. J. Park, T. A. Taton, C. A. Mirkin, *Science* **2002**, *295*, 1503–1506.
[3] A. T. Bell, *Science* **2003**, *299*, 1688–1691.
[4] M. H. Huang, S. Mao, H. Feick, H. Q. Yan, Y. Y. Wu, H. Kind, E. Weber, R. Russo, P. D. Yang, *Science* **2001**, *292*, 1897–1899.
[5] M. Law, H. Kind, B. Messer, F. Kim, P. D. Yang, *Angew. Chem.* **2002**, *114*, 2511–2514; *Angew. Chem. Int. Ed.* **2002**, *41*, 2405–2408.
[6] Y. G. Sun, Y. N. Xia, *Science* **2002**, *298*, 2176–2179.
[7] Y. D. Li, J. W. Wang, Z. X. Deng, Y. Y. Wu, X. M. Sun, D. P. Yu, P. D. Yang, *J. Am. Chem. Soc.* **2001**, *123*, 9904–9905.
[8] J. T. Hu, T. W. Odom, C. M. Lieber, *Acc. Chem. Res.* **1999**, *32*, 435–445.
[9] a) G. R. Patzke, F. Krumeich, R. Nesper, *Angew. Chem.* **2002**, *114*, 2554–2571; *Angew. Chem. Int. Ed.* **2002**, *41*, 2446–2461; b) J. Zygmunt, F. Krumeich, R. Nesper, *Adv. Mater.* **2003**, *15*, 1538–1541; c) F. Krumeich, H. J. Muhr, M. Niederberger, F. Bieri, B. Schnyder, R. Nesper, *J. Am. Chem. Soc.* **1999**, *121*, 8324–8331.
[10] See, for example: a special issue on nanowires: *Adv. Mater.* **2003**, *15*, 341–468.
[11] Y. Y. Wu, H. Q. Yan, M. Huang, B. Messer, J. H. Song, P. D. Yang, *Chem. Eur. J.* **2002**, *8*, 1260–1268.
[12] N. C. Seeman, *Nature* **2003**, *421*, 427–431.
[13] Y. N. Xia, P. D. Yang, *Adv. Mater.* **2003**, *15*, 351–352.
[14] Z. A. Peng, X. G. Peng, *J. Am. Chem. Soc.* **2001**, *123*, 1389–1395.
[15] Z. A. Peng, X. G. Peng, *J. Am. Chem. Soc.* **2002**, *124*, 3343–3353.
[16] W. W. Yu, X. G. Peng, *Angew. Chem.* **2002**, *114*, 2474–2477; *Angew. Chem. Int. Ed.* **2002**, *41*, 2368–2371.
[17] S. M. Lee, S. N. Cho, J. Cheon, *Adv. Mater.* **2003**, *15*, 441–444.
[18] X. G. Peng, *Adv. Mater.* **2003**, *15*, 459–463.
[19] C. F. Wu, W. P. Qin, G. S. Qin, D. Zhao, J. S. Zhang, S. H. Huang, S. Z. Lu, H. Q. Liu, H. Y. Lin, *Appl. Phys. Lett.* **2003**, *82*, 520–522.
[20] M. Yada, M. Mihara, S. Mouri, M. Kuroki, T. Kijima, *Adv. Mater.* **2000**, *12*, 309–313.
[21] X. Wang, Y. D. Li, *Angew. Chem.* **2002**, *114*, 4984–4987; *Angew. Chem. Int. Ed.* **2002**, *41*, 4790–4793.
[22] a) X. Wang, Y. D. Li, *Angew. Chem.* **2003**, *115*, 3654–3656; *Angew. Chem. Int. Ed.* **2003**, *42*, 3497–3500; b) X. Wang, X. M. Sun, D. P. Yu, B. S. Zhou, Y. D. Li, *Adv. Mater.* **2003**, *15*, 1442–1445; c) X. Wang, Y. D. Li, *Chem. Eur. J.* **2003**, *9*, 5627–5635.
[23] a) K. Riwotzki, H. Meyssamy, H. Schnablegger, A. Kornowski, M. Haase, *Angew. Chem.* **2001**, *113*, 574–578; *Angew. Chem. Int. Ed.* **2001**, *40*, 573–576; b) K. Riwotzki, H. Meyssamy, A. Kornowski, M. Haase, *J. Phys. Chem. B* **2000**, *104*, 2824–2828; c) P. Schuetz, F. Caruso, *Chem. Mater.* **2002**, *14*, 4509–4516; d) S. Nishihama, T. Hirai, I. Komasawa, *J. Mater. Chem.* **2002**, *12*, 1053–1057; e) S. Heer, O. Lehmann, M. Haase, H. U. Güdel, *Angew. Chem.* **2003**, *115*, 3288–3293; *Angew. Chem. Int. Ed.* **2003**, *42*, 3179–3182.
[24] H. Ito, Y. Fujishiro, T. Sato, A. Okuwaki, *Br. Ceram. Trans.* **1995**, *94*, 146–150.
[25] H. Meyssamy, K. Riwotzki, A. Kornowski, S. Naused, M. Haase, *Adv. Mater.* **1999**, *11*, 840–844.
[26] a) Y. J. Zhang, H. M. Guan, *J. Cryst. Growth* **2003**, *256*, 156–161; b) H. M. Guan, Y. J. Zhang, *J. Solid State Chem.* **2004**, *177*, 781–785.
[27] Y. P. Fang, A. W. Xu, R. Q. Song, H. X. Zhang, L. P. You, J. C. Yu, H. Q. Liu, *J. Am. Chem. Soc.* **2003**, *125*, 16025–16034.
[28] Y. W. Zhang, Z. G. Yan, L. P. You, R. Si, C. H. Yan, *Eur. J. Inorg. Chem.* **2003**, 4099–4104.
[29] Z. G. Yan, Y. W. Zhang, L. P. You, R. Si, C. H. Yan, *J. Cryst. Growth* **2004**, *262*, 408–414.
[30] M. S. Wickleder, *Chem. Rev.* **2002**, *102*, 2011–2087.
[31] Y. D. Li, X. L. Li, R. R. He, J. Zhu, Z. X. Deng, *J. Am. Chem. Soc.* **2002**, *124*, 1411–1416.
[32] X. Wang, Y. D. Li, *J. Am. Chem. Soc.* **2002**, *124*, 2880–2881.
[33] S. H. Yu, B. Liu, M. S. Mo, J. H. Huang, X. M. Liu, Y. T. Qian, *Adv. Funct. Mater.* **2003**, *13*, 639–647.
[34] X. Y. Gao, T. Gao, L. D. Zhang, *J. Mater. Chem.* **2003**, *13*, 6–8.
[35] W. O. Milligan, D. F. Mullica, G. W. Beall, L. A. Boatner, *Inorg. Chim. Acta* **1983**, *70*, 133–136.
[36] a) J. K. Bailey, C. J. Brinker, M. L. Mecartney, *J. Colloid Interface Sci.* **1993**, *157*, 1–13; b) A. Chemseddine, T. Moritz, *Eur. J. Inorg.*

Chem. **1999**, 235–245; c) Q. Peng, Y. J. Dong, Y. D. Li, *Inorg. Chem.* **2003**, *42*, 2174–2175.
[37] Z. T. Tang, N. A. Kotov, M. Giersig, *Science* **2002**, *297*, 237–240.
[38] Y. N. Xia, P. D. Yang, Y. G. Sun, Y. Y. Wu, B. Mayers, B. Gates, Y. D. Yin, F. Kim, H. Q. Yan, *Adv. Mater.* **2003**, *15*, 353–389.
[39] a) J. Yang, C. Xue, S. H. Yu, J. H. Zeng, Y. T. Qian, *Angew. Chem.* **2002**, *114*, 4891–4894; *Angew. Chem. Int. Ed.* **2002**, *41*, 4697–4700; b) J. Yang, J. H. Zeng, S. H. Yu, L. Yang, G. E. Zhou, Y. T. Qian, *Chem. Mater.* **2000**, *12*, 3259–3263.
[40] M. Yu, J. Lin, J. Fu, H. J. Zhang, Y. C. Han, *J. Mater. Chem.* **2003**, *13*, 1413–1419.
[41] a) H. E. Hoefdraad, *J. Solid State Chem.* **1975**, *15*, 175–177; b) Z. M. Qi, C. S. Shi, W. W. Zhang, W. P. Zhang, T. D. Hu, *Appl. Phys. Lett.* **2002**, *81*, 2857–2859; c) W. W. Zhang, W. P. Zhang, P. B. Xie, M. Yin, H. T. Chen, L. Jing, Y. S. Zhang, L. R. Lou, S. D. Xia, *J. Colloid Interface Sci.* **2003**, *262*, 588–593.
[42] J. Dexpert-Ghys, R. Mauricot, M. D. Faucher, *J. Lumin.* **1996**, *27*, 203–215.
[43] D. F. Mullica, W. O. Milligan, D. A. Grossie, G. W. Beall, L. A. Boatner, *Inorg. Chim. Acta* **1984**, *95*, 231–236.
[44] R. C. L. Mooney, *Acta Crystallogr.* **1950**, *6*, 337–340.
[45] W. O. Milligan, D. F. Mullica, G. W. Beall, L. A. Boatner, *Inorg. Chim. Acta* **1982**, *60*, 39–43.

Received: June 28, 2004
Revised: November 9, 2004
Published online: February 15, 2005

